Geophysical Research Letters

RESEARCH LETTER
10.1029/2024GL109271

Dynamic and Thermodynamic Control of the Response of Winter Climate and Extreme Weather to Projected Arctic Sea-Ice Loss

Kunhui Ye[1], Tim Woollings[1], and Sarah N. Sparrow[2]

[1]Atmospheric, Oceanic and Planetary Physics, University of Oxford, Oxford, UK, [2]Oxford e-Research Centre, Engineering Science, University of Oxford, Oxford, UK

Key Points:

- A novel sub-sampling method is introduced to isolate the role of dynamics in the response to projected Arctic sea-ice loss
- A dynamical Siberian High response dominates the temperature response over East Eurasia while that of the North Atlantic Oscillation is weak
- Inter-model differences in Polar Amplification Model Intercomparison Project likely contain a large fraction of internal variability due to the unconstrained dynamic effects

Supporting Information:

Supporting Information may be found in the online version of this article.

Correspondence to:

K. Ye,
kunhui.ye@physics.ox.ac.uk

Citation:

Ye, K., Woollings, T., & Sparrow, S. N. (2024). Dynamic and thermodynamic control of the response of winter climate and extreme weather to projected Arctic sea-ice loss. *Geophysical Research Letters*, *51*, e2024GL109271. https://doi.org/10.1029/2024GL109271

Received 27 MAR 2024
Accepted 19 JUN 2024

Abstract A novel sub-sampling method has been used to isolate the dynamic effects of the response of the North Atlantic Oscillation (NAO) and the Siberian High (SH) from the total response to projected Arctic sea-ice loss under 2°C global warming above preindustrial levels in very large initial-condition ensemble climate simulations. Thermodynamic effects of Arctic warming are more prominent in Europe while dynamic effects are more prominent in Asia/East Asia. This explains less-severe cold extremes in Europe but more-severe cold extremes in Asia/East Asia. For Northern Eurasia, dynamic effects overwhelm the effect of increased moisture from a warming Arctic, leading to an overall decrease in precipitation. We show that the response scales linearly with the dynamic response. However, caution is needed when interpreting inter-model differences in the response because of internal variability, which can largely explain the inter-model spread in the NAO and SH response in the Polar Amplification Model Intercomparison Project.

Plain Language Summary The projected loss of Arctic sea-ice under 2°C global warming will cause large warming in the Arctic region and climate and weather anomalies outside the Arctic. The warming in the Arctic will mean warmer airmasses coming from the Arctic and also more moisture from the open Arctic Ocean. Furthermore, it will also change atmospheric circulation. These effects together will determine the impacts of Arctic warming. In this study, we introduce a novel sub-sampling method to isolate atmospheric circulation change in response to the Arctic warming. The method involves selecting members of simulations from the experiment with future Arctic sea-ice conditions, the average of which is equal to the average of the members of simulations in the experiment with present-day Arctic sea-ice conditions. We found that atmospheric circulation change in European regions is relatively weak so that warming effects will dominate the climate and weather response there. On the other hand, atmospheric circulation change will dominate the climate and weather response in East Eurasia. We also found that stronger atmospheric circulation changes will generally increase the response to the Arctic warming. We suggest caution when assessing whether different responses in different models can be interpreted as true differences in model physics.

1. Introduction

Arctic sea-ice loss and Arctic amplification of warming (AA) under global climate change have been thought to drive midlatitude climate and weather changes (Cohen et al., 2014, 2020; Francis & Vavrus, 2015; Mori et al., 2014; Screen & Simmonds, 2010). This however remains contentious. Contrasting opinions are present, for example, on driving of the recent winter Eurasian cooling trends and cold extremes by AA (Tang et al., 2013; Wu et al., 2017; Zhang et al., 2018; Ye & Messori, 2020; Outten et al., 2023 and references therein). The purported influence of Arctic sea-ice loss on European cold extremes (e.g., Petoukhov & Semenov, 2010; Yang & Christensen, 2012) is not found in many studies (Blackport et al., 2019; Screen, 2017; Woollings et al., 2014). It is suggested that moisture from Arctic sea-ice loss leads to more snowfall (Liu et al., 2012) and extreme European snowfall (Bailey et al., 2021). It is still, however, quantitatively unclear how dynamics and thermodynamics compare to each other in shaping the impacts of Arctic sea-ice loss. Quantifying their relative importance will help better understand the response to Arctic sea-ice loss and AA. Climate modeling has established causality in Arctic sea-ice and AA impacts but model uncertainty and internal variability have obfuscated our understanding. Recent comprehensive climate modeling work including the Polar Amplification Model Intercomparison Project (PAMIP; Smith et al., 2022) and the very large-ensemble climate simulations (Ye et al., 2024) has shed much light on Arctic sea-ice loss impacts. In particular, due to the sheer number of ensemble members, the very large-

ensemble climate simulations provide a unique opportunity to isolate the dynamical response to improve understanding of these impacts.

In this study, we apply a novel sub-sampling method to the very large-ensemble climate simulations to isolate dynamic effects of specifically the North Atlantic Oscillation (NAO) and the Siberian High (SH) from the total response to projected Arctic sea-ice loss. These are usually the most prominent features of atmospheric circulation response to projected Arctic sea-ice loss (Smith et al., 2022; Ye et al., 2024). Such a sub-sampling method is usually not possible for small ensemble climate modeling including individual models in the PAMIP. Previous studies have adopted linear frameworks to isolate dynamic effects (Screen, 2017; Ye et al., 2023; Zheng et al., 2023) or used sub-sampling (Sun et al., 2022) to study stratospheric internal variability in the response to Arctic sea-ice loss. Our sub-sampling method does not assume linearity but will test it by sub-sampling. We compare dynamic effects of the NAO and SH response to the full response to discuss, and quantify, the sensitivity of the response to these dynamic effects. We further discuss whether the inter-model difference in the PAMIP could be largely due to internal variability and implications for constraining model response to projected Arctic sea-ice loss.

2. Data and Methodology

2.1. PAMIP Data

Details of the PAMIP data can be found in Smith et al. (2022). The two atmosphere-only experiments prescribed with ocean surface boundary conditions and run with >=100 14-month members, namely pdSST-pdSIC and pdSST-futArcSIC, are used to obtain the total response to projected Arctic sea-ice loss under a 2°C global warming. Present-day sea surface temperatures (SSTs) and Antarctic sea-ice concentrations are prescribed in both experiments. Present-day (future) Arctic sea-ice is prescribed in pdSST-pdSIC (pdSST-futArcSIC) with corresponding future Arctic SSTs also prescribed if Arctic sea-ice loss is over 10%. Note that greenhouse gases are kept at present-day levels, so that these experiments test the response to Arctic sea ice loss in isolation of global warming.

2.2. Very Large-Ensemble HadAM4 Climate Model Simulations

These model simulations adopt the same experimental design and use the same ocean surface boundary conditions as in the PAMIP for the two atmosphere-only experiments (pdSST-pdSIC and pdSST-futArcSIC). However, they are run on the University of Oxford's innovative distributed computing project (Climateprediction.net) with many ensemble members and for two different resolutions. Specifically, these simulations include a ∼2,200 member ensemble of 13-month simulations from October run with the lower-resolution version (∼90 km, N144) of Met Office Hadley Centre global atmospheric model Version 4 (HadAM4) and a ∼1,500 member ensemble of 5-month simulations from November run with the higher-resolution version (∼60 km, N216). Details of these simulations can be found in Ye et al. (2024). Winter is defined as the months of December, January and February throughout the paper.

2.3. Definitions of Atmospheric Circulation Indices and Diagnostic Metrics, and Domains for Computing Area Means

The square-root of the cosine of the latitude is used for weighting for all area-mean computations. The NAO is defined as the difference between area-mean SLP over the Azores (28–20°W, 36–40°N) and Iceland (25–16°W, 63–70°N). The SH is defined as the area-mean SLP over the domain of 80–120°E, 40–65°N. Daily zonal wind at 850 hPa over the domain of 60°W–0°E, 15°N–75°N was used to compute the two jet indices—latitude and speed—for the North Atlantic Jet (Woollings et al., 2010). Similar procedures are followed to compute jet indices for the East Asian jet except that the domain is changed to 120°E–180°E, 20°N–40°N using daily zonal wind at 250 hPa. Storm track activity is measured by the variance of 2.5–6-day band-pass filtered meridional wind at 250 hPa. Extreme temperature is defined as the first percentile of the daily temperature distribution. Domains for computing the area-mean for different variables are summarized in Table S1 in Supporting Information S1.

2.4. Sub-Sampling Method for Isolating Dynamics of NAO and SH Contributing to the Total Response

The major idea is to find large-ensemble sub-samples in pdSSt-furArcSIC which have similar NAO/SH climatology to the pdSST-pdSIC experiment. The difference between these sub-samples and the pdSST-pdSIC

experiment is considered to have no dynamic effects of the NAO/SH response. First, a reference NAO/SH climatology is defined in pdSST-pdSIC using the above definitions. Second, a random sub-sample of 400-member size without replacement is randomly drawn from the pool of large ensembles in pdSST-futArcSIC, and the sub-sample is retained if the average of the NAO/SH indices is similar to the reference NAO/SH climatology, with a margin of −0.01 to 0.01 hPa. The use of a 400-member ensemble size helps to suppress internal variability while still limiting the potential overlapping between sub-samples. The random selection process is realized by first randomly reordering the entire pool of large ensembles before selecting the first 400 ensembles. This process is repeated 1,500 times to obtain as many unique sub-samples as possible but further repetitions are increasingly difficult given the above-mentioned criteria. Finally, the average of the differences in variables of interest taken between each of the sub-samples and the pdSST-pdSIC experiment is defined as the non-NAO/SH response; the dynamical effects of the NAO/SH are obtained by subtracting the non-NAO/SH response from the total response using all ensembles. While the non-NAO/SH response does not necessarily equate to thermodynamic effects, it reflects mainly the thermodynamic warming/moistening effect of Arctic sea-ice loss in many cases.

To remove both the dynamic effects of the NAO and SH in the total response, the NAO response is subtracted from the non-SH response, as the NAO and SH responses are mostly independent from each other. Further discussions on this are provided in Text S1 and Figure S1 in Supporting Information S1 and also in Section 3.1.

2.5. Sub-Sampling Method for Quantifying the Sensitivity of the Response for Different Magnitudes of the NAO and SH Response

A reference NAO/SH response is defined as the response obtained using all available ensembles in the pdSST-futArcSIC and pdSST-pdSIC experiments. This reference NAO/SH response is also referred to as one unit of NAO/SH response. A sub-sampling method is used to randomly draw a pair of sub-samples of 400-member size without replacement from the two experiments respectively. The random drawing process is the same as in Section 2.4. The pair of sub-samples is retained if the NAO/SH response falls within each of the groups that have either 0.5, 1, 1.5 or 2 times the reference NAO/SH response, with a margin of −0.01 to 0.01 hPa. Each pair of sub-samples is unique within each group. The difference in variables of interest between the pair of sub-samples is taken to be the response. This sub-sampling procedure is also repeated 1,500 times. The change of the response of different variables for an increase of one unit of NAO/SH response is computed as follows. First, the differences in the averages of response between the groups with 1, 1.5 or 2 times the reference NAO/SH response, and that with half of the reference NAO/SH response are computed, with the differences for the second and third groups divided by 2 and 3 respectively. Second, these differences are averaged and the obtained average is multiplied by 2 to obtain the required value.

3. Results

3.1. Spatial Distribution of Dynamical Versus Remaining Contributions to Total Response

The low pressure anomaly in the North Atlantic associated to the NAO response dominates the total response (Figure 1a and Figure S2a in Supporting Information S1). The NAO response captures most of the North Atlantic jet latitude response and around 63% of the jet speed response (Figure 2a). The non-NAO response is characterized by low pressure anomalies over regions with strongest sea-ice loss and high-pressure anomalies over Northern Eurasia (Figure 1c). The NAO response thus represents a mostly localized dynamical response over the North Atlantic-European sector. However, it corresponds to a large-scale response in storm track activity with a dipole of response in the North Pacific and North Atlantic (Figure 1f). The NAO response explains around 65% of the storm track response in the North Atlantic-European region (Figure 2a). There is a considerable non-NAO response in the storm track activity (Figure 1h).

The SH response captures well the high-pressure anomaly situated in Northern Eurasia (Figure 1b) and the East Asian jet speed increase (Figure 2b). In terms of storm track response, there is a belt of decreasing activity from the North Atlantic across Northern Eurasia to the North Pacific (Figure 1g). The SH response explains roughly 37% of the storm track activity response in Northern Eurasia (Figure 2b). Again, the non-SH response is considerable (Figure 1i). The NAO response is not linked much to the SH response, instead projecting onto the non-SH response (Figure 1d). By removing both the NAO and SH response, we can see the signature of "heat lows" over the specific regions with sea-ice loss (Figure 1e; Woollings et al., 2023). The decrease in storm track

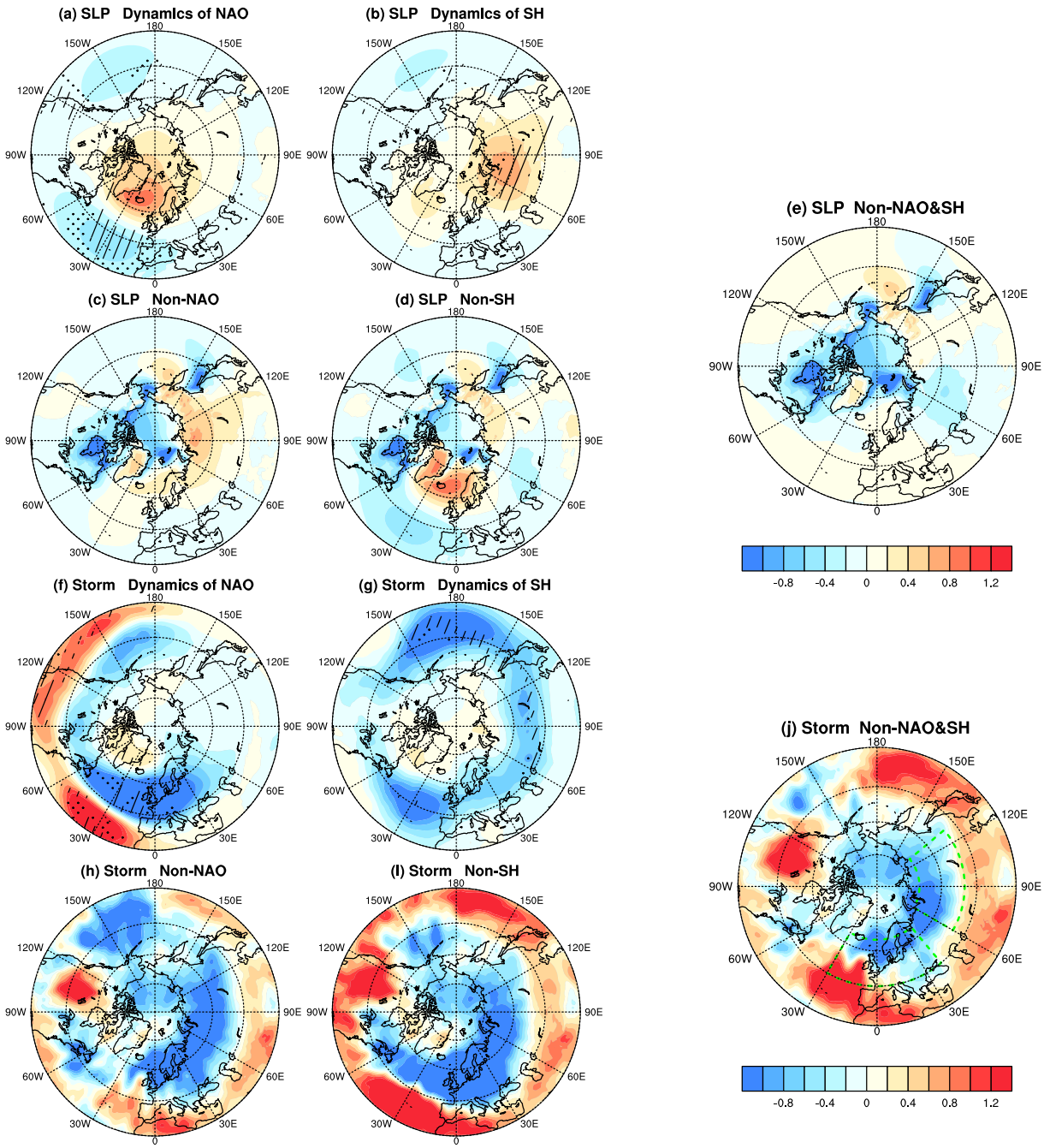

Figure 1. Dynamical effects of the NAO and SH and other effects not-related to them for N144. (a, b) SLP response associated to the NAO and SH dynamic response and (c, d) Non-NAO/SH response. (f, g) Storm track activity response associated to the NAO and SH response and (h, i) Non-NAO/SH response. (e) SLP response after removing both the NAO and SH dynamic response. (j) Same as in (e) but for storm track activity. Dots indicate that dynamics effect accounts for >=80% of the total response; slashes indicate that dynamic effect is >=80% larger than the Non-NAO/SH response in absolute value when they are of opposite signs. Green dashed polygons denote the domains for computing area-mean. Units: hPa and m^2/s^2 for SLP and storm track activity, respectively.

activity over Northern Eurasia is likely caused by the reduced baroclinicity at high latitudes, while increased activity is seen further south (Figure 1j). Similar features are broadly seen in N216 though some differences are noted (Figure S3 in Supporting Information S1).

Having seen the dynamical NAO/SH response versus non-NAO/SH response, we now turn to their influence on the surface climate response (Figure 3). The remaining response (i.e., Non-NAO, Non-SH and Non-NAO&SH) after

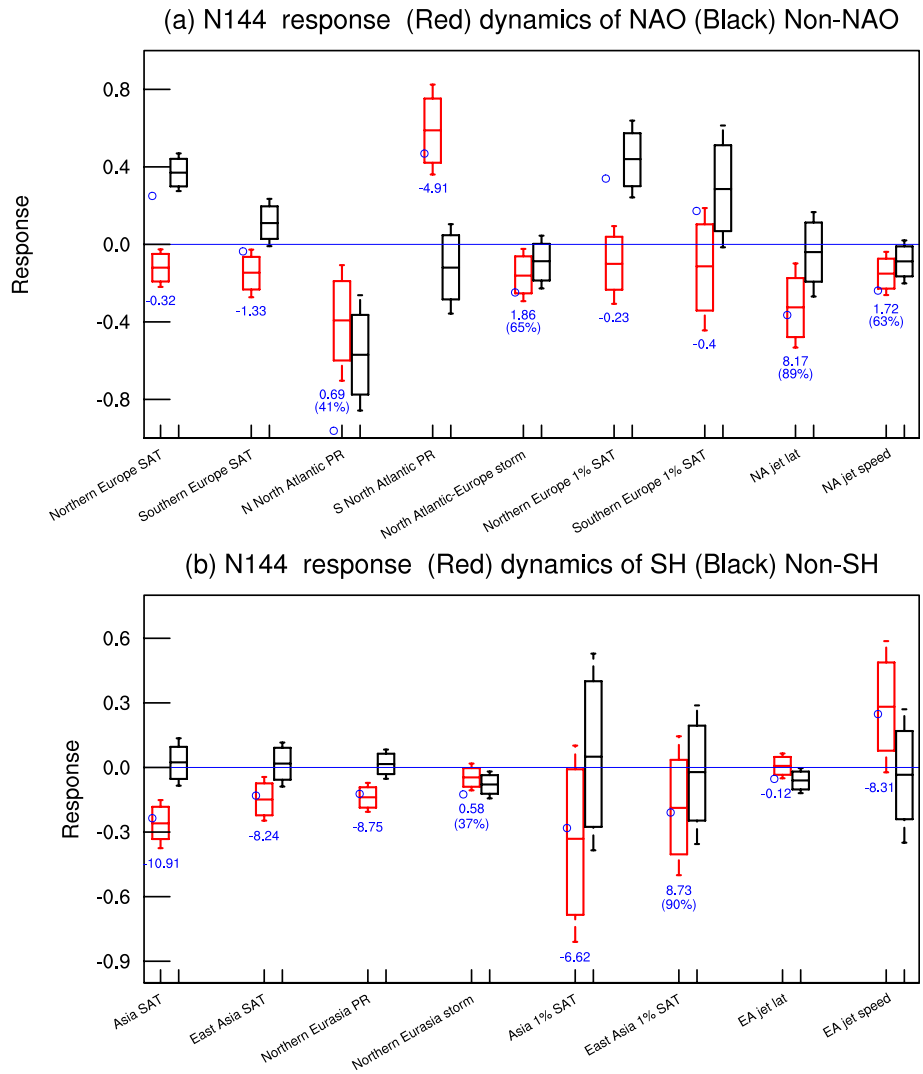

Figure 2. (a) (red) Dynamic effect of the NAO and (black) Non-NAO effect. (b) (red) Dynamic effect of the SH and (black) Non-SH effect. Blue numbers show values obtained by dividing dynamic effect of NAO/SH by Non-NAO/SH effect, which measure their relative magnitudes. The percentage of total response explained by dynamic effect is given if dynamic effect of NAO/SH and Non-NAO/SH effect have the same sign. Shown in the boxplots are minimum, lower 5%, average, upper 95% and maximum values. Precipitation and storm track activity are divided by 10. Units: °C for temperature, mm/season for precipitation, m^2/s^2 for storm track activity, degrees latitude for jet latitude and m/s for jet speed.

removing the NAO and/or SH response is associated to warmer Arctic airmasses (Figures 3c–3e). The NAO response induces cooling over Northern Eurasia and eastern North America, and warming over Canada/Greenland and North Africa (Figure 3a). The non-NAO response, associated to warmer Arctic airmass (Figure 3c), dominates the temperature response in Northern Europe but is roughly offset in southern Europe (Figure 2a). However, for temperature extremes, the non-NAO response (favoring less severe extremes) dominates over the NAO response (favoring more-severe extremes), leading to less-severe extremes for both southern and northern Europe (Figure 2a). These are mostly consistent with a previous study (Screen, 2017). The SH response induces a large cooling response in Eastern Eurasia (Figure 3b) and dominates for both seasonal and extreme temperature responses (Figure 2b).

The NAO response explains 41% of the precipitation response in the northern part of the North Atlantic (Figures 1f and 3f) and explains 65% of the storm track response over North Atlantic-Europe (Figure 2a). The major effect of the SH response is a decrease in precipitation in Northern Eurasia (Figures 2b and 3g). The remaining response after removing NAO or SH is characterized by large precipitation increases but these are very

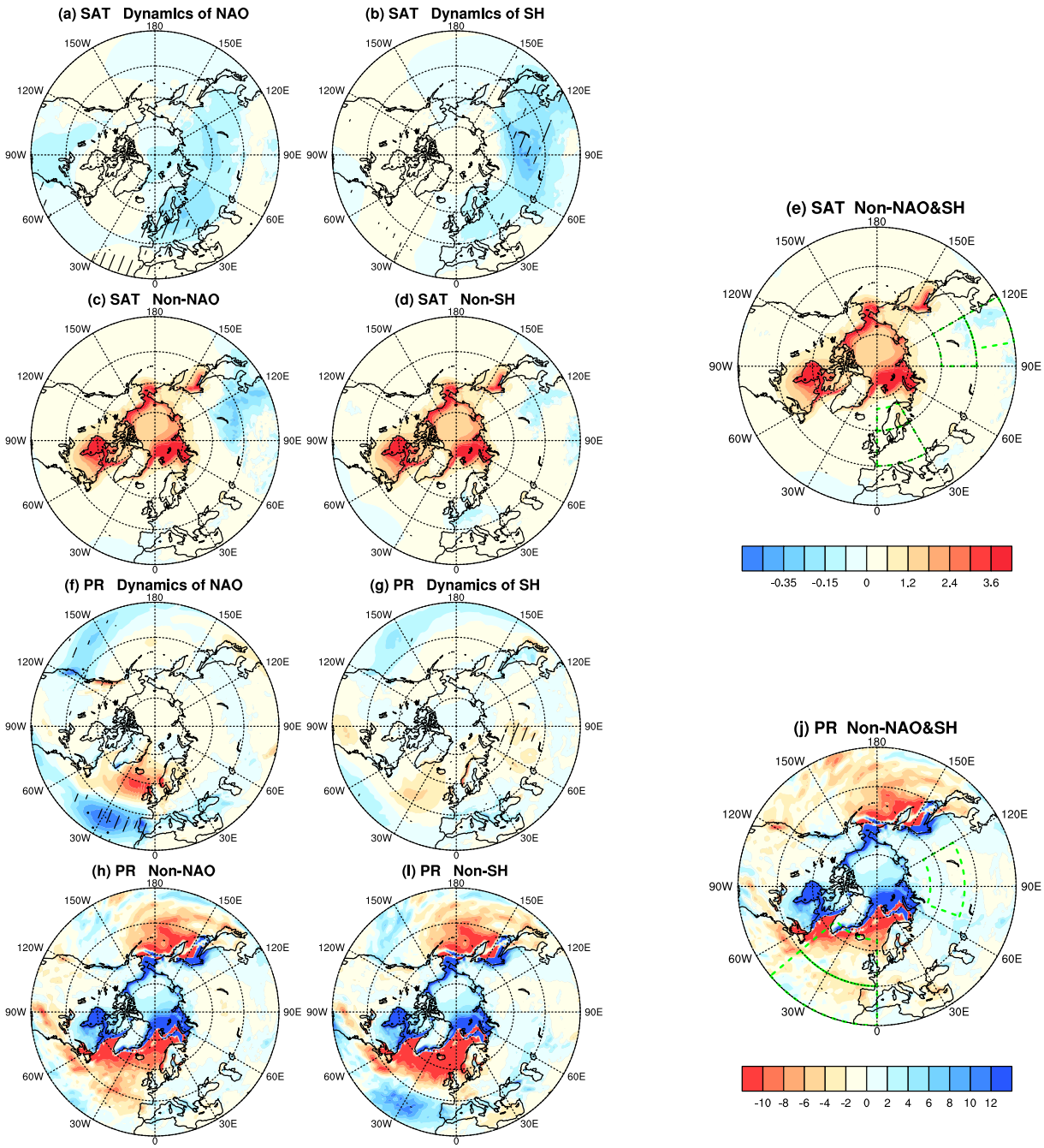

Figure 3. Similar to Figure 1 but for (a–d) SAT and (f–i) precipitation. (e) SAT response after removing both the NAO and SH response. (j) Same as in (e) but for precipitation. Units: °C for temperature and mm/season for precipitation.

localized to the oceanic regions of imposed sea-ice loss (Figures 3h and 3i). After removing both the NAO and SH responses, there is a positive precipitation response in Northern Eurasia particularly in western Russia (Figure 3j). This is consistent with the expected increase in moisture from the Arctic sea-ice loss. This effect, however, seems to be weak compared to the dynamical effects which reduce storm track activity (Figures 1g and 2b) and lead to a negative total precipitation response in Northern Eurasia (Figure S2g in Supporting Information S1).

Similar features are seen in N216, suggesting the consistency between resolutions but some differences are noted (Figures S4 and S5; Text S2 in Supporting Information S1).

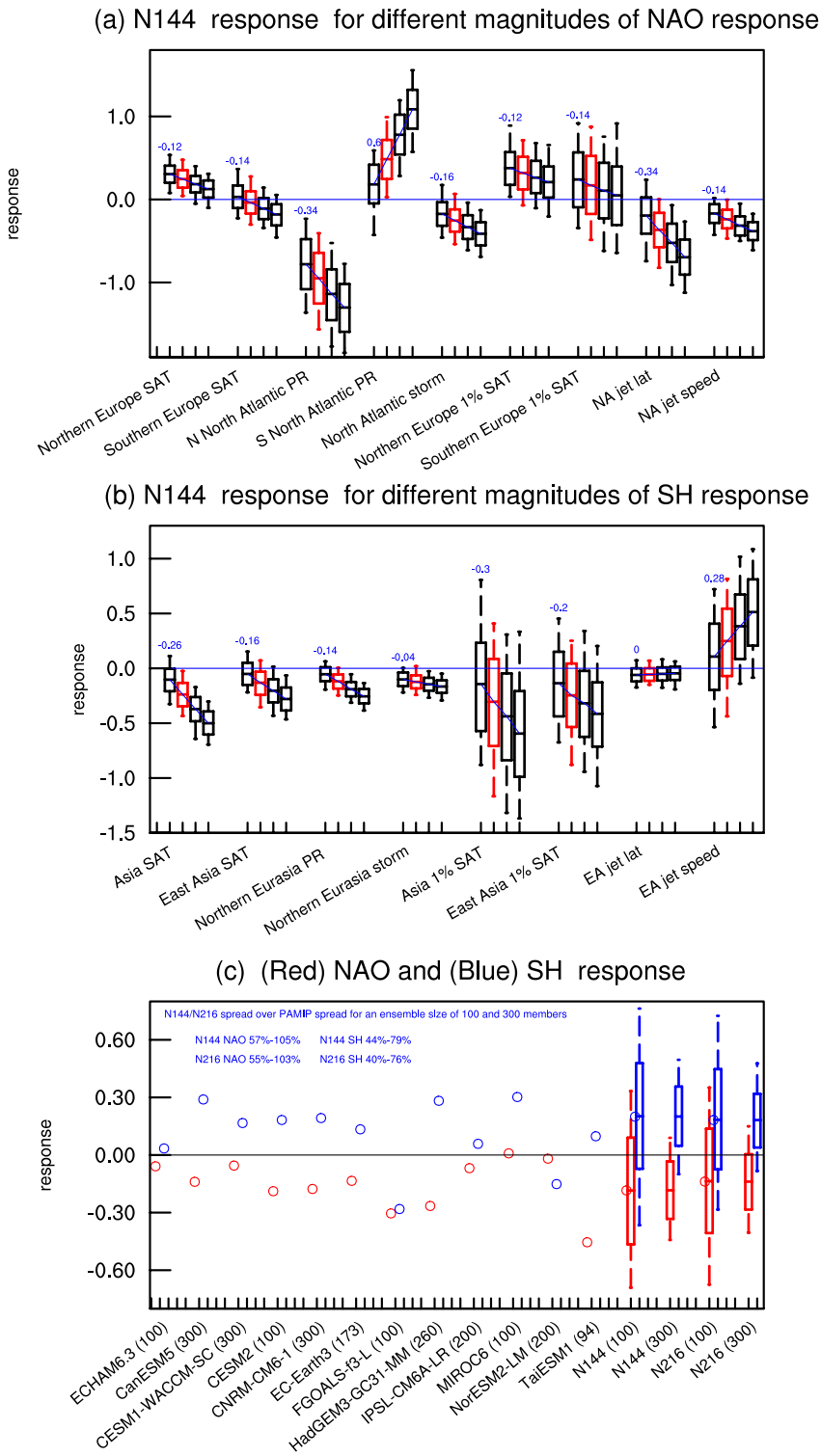
(a) N144 response for different magnitudes of NAO response
response
1.0
0.0
-1.0
-0.12
-0.14
-0.34
-0.16
-0.12
-0.14
-0.34
-0.14
Northern Europe SAT
Southern Europe SAT
N North Atlantic PR
S North Atlantic PR
North Atlantic storm
Northern Europe 1% SAT
Southern Europe 1% SAT
NA jet lat
NA jet speed
(b) N144 response for different magnitudes of SH response
response
1.0
0.5
0.0
-0.5
-1.0
-1.5
-0.26
-0.16
-0.14
-0.04
-0.3
-0.2
0
0.28
Asia SAT
East Asia SAT
Northern Eurasia PR
Northern Eurasia storm
Asia 1% SAT
East Asia 1% SAT
EA jet lat
EA jet speed
(c) (Red) NAO and (Blue) SH response
N144/N216 spread over PAMIP spread for an ensemble size of 100 and 300 members
N144 NAO 57%-105%
N144 SH 44%-79%
N216 NAO 55%-103%
N216 SH 40%-76%
response
0.60
0.30
0.00
-0.30
-0.60
ECHAM6.3 (100)
CanESM5 (300)
CESM1-WACCM-SC (300)
CESM2 (100)
CNRM-CM6-1 (300)
EC-Earth3 (173)
FGOALS-f3-L (100)
HadGEM3-GC31-MM (260)
IPSL-CM6A-LR (200)
MIROC6 (100)
NorESM2-LM (200)
TaiESM1 (94)
N144 (100)
N144 (300)
N216 (100)
N216 (300)

Figure 4.

3.2. Sensitivity of Climate and Extremes Response to Different Magnitudes of NAO and SH Response

The dynamic response of the NAO and SH may be model-dependent and this would thus translate into varied dynamic contributions to the response, with potentially a large impact on extremes. One important question is thus how sensitive is the response of both mean climate and extremes to changes in the dynamic response of the NAO and SH? To answer this question, we compare these responses between different magnitudes of the NAO and SH response using the sub-sampling method in Section 2.5 (Figure 4).

Overall, the response is found to scale mostly linearly with the magnitude of the NAO (Figure 4a) and SH (Figure 4b) responses as shown by the blue numbers and lines (see the figure caption for details), and interestingly this is true for changes in extremes as well as means. For a doubled NAO response, seasonal warming in Northern Europe is still significant but the cooling response in southern Europe emerges as a robust signal. Also for doubled NAO response, less-severe temperature extremes in Northern Europe are still the dominant response as the thermodynamic warming effect is strong (see Figure 2a); however, the temperature extremes response in southern Europe becomes relatively small and uncertain owing to the tug of war between dynamics and thermodynamics. This suggests that more-severe cold extremes in southern Europe are not very likely, even in response to sea-ice loss in isolation of global warming. For precipitation, increasing the NAO response will enhance the dipole precipitation response (see Figure 2a).

For increasing magnitudes of SH response, this will strengthen the already-strong dynamic effects of SH response (except for the weak East Asian jet latitude response; Figure 4b). The impact on the seasonal and extreme temperature is larger for Asia than for East Asia as the dynamic effects of the SH response are stronger in Asia. The results for N216 are mostly similar to N144 (Figure S6 in Supporting Information S1).

3.3. Inter-Model Difference in the NAO and SH Response in the PAMIP and Role of Internal Variability

Assuming similar Arctic warming induced by sea-ice loss, our results suggest that models which have larger dynamic responses of the NAO and SH are likely to feature stronger responses for many variables. The PAMIP has multimodel ensembles which allows for quantifying inter-model difference in the response to projected Arctic sea-ice loss. If some metrics can be closely linked to NAO/SH this may provide a reliable way to constrain the response to projected Arctic sea-ice loss.

The NAO/SH response from both the PAMIP and the very large-ensemble simulations (red and blue circles), and distributions of sub-sampled responses (red and blue boxplots) are displayed in Figure 4c. Note that the responses are divided by the standard deviation of the NAO/SH indices for the pdSST-pdSIC experiment to normalize the variability across models. Model-spread in the PAMIP and inter-sample spread are defined by standard deviation across models/sub-samples. The NAO/SH response in the PAMIP does exhibit considerable inter-model difference. The actual member size available for computing the response of NAO/SH indices in the PAMIP ranges from 94 to 300, with five models having an ensemble size of 100 or less. To explain the inter-model difference, we construct the lower bound and upper bound estimates of spread in the PAMIP due to internal variability (blue text in Figure 4c) using the sub-sampling method for an ensemble size of 300 and 100 members respectively. A brief discussion on internal variability represented in individual PAMIP models and in the very large-ensemble climate simulations is provided in Text S3 and Figure S7 in Supporting Information S1. Similar methods have been used previously to explain inter-model spread (Deser et al., 2012; Ye & Messori, 2021). For the upper bound estimate, the NAO/SH response in all the PAMIP models falls within the range of the sub-sampled response in N144. This is true for most of the PAMIP models even for the lower bound estimate in N144. A similar situation is observed

Figure 4. Response to projected Arctic sea-ice loss computed for an ensemble size of 400 for different magnitudes of the NAO (hPa) and SH (hPa) response for N144, and the response of NAO and SH in the PAMIP and sub-sampled (100/300-member without replacement) from the very large-ensemble climate simulations. (a) Boxplot of response for different magnitude of the NAO response, equating respectively to 0.5, (red) 1, 1.5 and 2 times that using all available ensembles (defined as per unit of NAO/SH response). (b) As in (a) but for SH. Blue numbers show the change of the response of different variables for an increase of one unit of NAO/SH response. Blue lines linking the averages of the responses in each group are also shown. (c) Normalized (red circles) NAO and (blue circles) SH responses computed for the PAMIP and those using the very large-ensemble climate simulations. The ensemble size for each PAMIP model is given. Sub-sampled response of the (red) NAO and (blue) SH with 10,000 repetitions is displayed for both N144 and N216. Blue text at the top shows the ratio of sub-sampled spread to the inter-model spread in the PAMIP for an ensemble size of 100 and of 300, respectively, for upper and lower bound estimates. Values shown in the boxplots are the same as in Figure 2. Precipitation and storm track activity are divided by 10. Units: °C for temperature, mm/season for precipitation, m^2/s^2 for storm track activity, degrees latitude for jet latitude and m/s for jet speed.

for N216 though the SH response for FGOALS-f3-L lies outside the range for the lower bound estimate in N216. The fraction of explained inter-model spread in the PAMIP by internal variability is from 57% to 105% for the NAO response between the lower bound and upper bound estimates for N144 while it is from 43% to 79% for the SH response. The corresponding value is from 55% to 103% for the NAO response and from 40% to 76% for the SH response for N216. This suggests that inter-model difference in the PAMIP response (pdSST-futArcSIC minus pdSST-pdSIC) is likely largely due to internal variability, and hence constraining the response to Arctic sea ice loss using these experiments may not be recommended.

4. Discussion and Conclusions

We note that extratropical ocean warming may enhance the response to Arctic sea-ice loss (Blackport & Kushner, 2018) but equally coupled internal variability may confound the detection of true response (Peings et al., 2021). We have successfully used a novel sub-sampling method to isolate specifically the dynamical effects of the NAO and SH from the total response to projected Arctic sea-ice loss to help to better understand the response and inter-model difference.

In general, compared to other factors including the direct thermodynamic effects of Arctic warming, the dynamic effect of the NAO is less pronounced in Europe but the dynamic effect of the SH is generally dominant for Asia/East Asia. A warming Arctic is not found to induce more cold extremes in Europe or to induce more precipitation in Northern Eurasia. For extreme temperature responses in Europe, a dynamical NAO response of the magnitude required to overcome the thermodynamic warming is not very likely. For the precipitation response in Northern Eurasia, the dynamical response generally cancels out the expected effect of increased moisture from a warming Arctic, and a decrease in total precipitation response is thus seen. Our analysis does support that Arctic sea-ice loss in isolation of global warming would induce more cold extremes in Asia and particularly East Asia, attributed to strong dynamic effects.

The response to projected Arctic sea-ice loss is found to scale linearly with the response of the NAO and SH. This does suggest potential model dependence of response if the response is well separated from internal variability. The inter-model difference in the PAMIP in terms of the NAO and SH response is found to be largely internal variability driven. This is consistent with a previous study that suggests that inter-model differences could not be separated from internal variability in the PAMIP (Zheng et al., 2023). Constraining the response to Arctic sea ice loss using these metrics may not be recommended in the PAMIP.

Data Availability Statement

The PAMIP data can be freely downloaded from https://esgf-node.llnl.gov/search/cmip6/ by selecting "PAMIP" activity. The very large-ensemble climate simulations are not publicly available due to ongoing work to create a permanent data deposition at the Centre for Environmental Data Analysis (https://www.ceda.ac.uk/), but are available from the corresponding author on reasonable request.

Acknowledgments
K.Y., T.W., and S.N.S., were supported by the UK NERC Project NE/V005855/1. This research was funded in whole, or in part, by the UKRI [NE/V005855/1]. K.Y. also acknowledges the support of the UKRI Horizon Europe Guarantee MSCA Postdoctoral Fellowship EP/Y029119/1. The contents reflect only the author's views and not the views of the UKRI. For the purpose of Open Access, the author has applied a CC BY public copyright license to any Author Accepted Manuscript version arising from this submission.

References

Bailey, H., Hubbard, A., Klein, E. S., Mustonen, K. R., Akers, P. D., Marttila, H., & Welker, J. M. (2021). Arctic sea-ice loss fuels extreme European snowfall. *Nature Geoscience*, *14*(5), 283–288. https://doi.org/10.1038/s41561-021-00719-y

Blackport, R., & Kushner, P. J. (2018). The role of extratropical ocean warming in the coupled climate response to Arctic sea ice loss. *Journal of Climate*, *31*(22), 9193–9206. https://doi.org/10.1175/jcli-d-18-0192.1

Blackport, R., Screen, J. A., van der Wiel, K., & Bintanja, R. (2019). Minimal influence of reduced Arctic sea ice on coincident cold winters in mid-latitudes. *Nature Climate Change*, *9*(9), 697–704. https://doi.org/10.1038/s41558-019-0551-4

Cohen, J., Screen, J. A., Furtado, J. C., Barlow, M., Whittleston, D., Coumou, D., et al. (2014). Recent Arctic amplification and extreme mid-latitude weather. *Nature Geoscience*, *7*(9), 627–637. https://doi.org/10.1038/NGEO2234

Cohen, J., Zhang, X., Francis, J., Jung, T., Kwok, R., Overland, J., et al. (2020). Divergent consensuses on Arctic amplification influence on midlatitude severe winter weather. *Nature Climate Change*, *10*(1), 20–29. https://doi.org/10.1038/s41558-019-0662-y

Deser, C., Phillips, A., Bourdette, V., & Teng, H. (2012). Uncertainty in climate change projections: The role of internal variability. *Climate Dynamics*, *38*(3–4), 527–546. https://doi.org/10.1007/s00382-010-0977-x

Francis, J. A., & Vavrus, S. J. (2015). Evidence for a wavier jet stream in response to rapid Arctic warming. *Environmental Research Letters*, *10*(1), 014005. https://doi.org/10.1088/1748-9326/10/1/014005

Liu, J., Curry, J. A., Wang, H., Song, M., & Horton, R. M. (2012). Impact of declining Arctic sea ice on winter snowfall. *Proceedings of the National Academy of Sciences*, *109*(11), 4074–4079. https://doi.org/10.1073/pnas.1114910109

Mori, M., Watanabe, M., Shiogama, H., Inoue, J., & Kimoto, M. (2014). Robust Arctic sea-ice influence on the frequent Eurasian cold winters in past decades. *Nature Geoscience*, *7*(12), 869–873. https://doi.org/10.1038/ngeo2277

Outten, S., Li, C., King, M. P., Suo, L., Siew, P. Y., Cheung, H., et al. (2023). Reconciling conflicting evidence for the cause of the observed early 21st century Eurasian cooling. *Weather and Climate Dynamics*, *4*(1), 95–114. https://doi.org/10.5194/wcd-4-95-2023

Peings, Y., Labe, Z. M., & Magnusdottir, G. (2021). Are 100 ensemble members enough to capture the remote atmospheric response to + 2°C Arctic sea ice loss? *Journal of Climate*, *34*(10), 3751–3769. https://doi.org/10.1175/JCLI-D-20-0613.1

Petoukhov, V., & Semenov, V. A. (2010). A link between reduced Barents-Kara sea ice and cold winter extremes over northern continents. *Journal of Geophysical Research*, *115*(D21), D21111. https://doi.org/10.1029/2009jd013568

Screen, J. A. (2017). The missing Northern European winter cooling response to Arctic sea ice loss. *Nature Communications*, *8*(1), 14603. https://doi.org/10.1038/ncomms14603

Screen, J. A., & Simmonds, I. (2010). The central role of diminishing sea ice in recent arctic temperature amplification. *Nature*, *464*(7293), 1334–1337. https://doi.org/10.1038/nature09051

Smith, D. M., Eade, R., Andrews, M. B., Ayres, H., Clark, A., Chripko, S., et al. (2022). Robust but weak winter atmospheric circulation response to future Arctic sea ice loss. *Nature Communications*, *13*(1), 1–15. https://doi.org/10.1038/s41467-022-28283-y

Sun, L., Deser, C., Simpson, I., & Sigmond, M. (2022). Uncertainty in the winter tropospheric response to Arctic Sea ice loss: The role of stratospheric polar vortex internal variability. *Journal of Climate*, *35*(10), 3109–3130. https://doi.org/10.1175/jcli-d-21-0543.1

Tang, Q., Zhang, X., Yang, X., & Francis, J. A. (2013). Cold winter extremes in northern continents linked to Arctic sea ice loss. *Environmental Research Letters*, *8*(1), 014036. https://doi.org/10.1088/1748-9326/8/1/014036

Woollings, T., Hannachi, A., & Hoskins, B. (2010). Variability of the North Atlantic eddy-driven jet stream. *Quarterly Journal of the Royal Meteorological Society*, *136*(649), 856–868. https://doi.org/10.1002/qj.625

Woollings, T., Harvey, B., & Masato, G. (2014). Arctic warming, atmospheric blocking and cold European winters in CMIP5 models. *Environmental Research Letters*, *9*(1), 014002. https://doi.org/10.1088/1748-9326/9/1/014002

Woollings, T., Li, C., Drouard, M., Dunn-Sigouin, E., Elmestekawy, K. A., Hell, M., et al. (2023). The role of Rossby waves in polar weather and climate. *Weather and Climate Dynamics*, *4*(1), 61–80. https://doi.org/10.5194/wcd-4-61-2023

Wu, B., Yang, K., & Francis, J. A. (2017). A cold event in Asia during January–February 2012 and its possible association with Arctic sea ice loss. *Journal of Climate*, *30*(19), 7971–7990. https://doi.org/10.1175/jcli-d-16-0115.1

Yang, S., & Christensen, J. H. (2012). Arctic sea ice reduction and European cold winters in CMIP5 climate change experiments. *Geophysical Research Letters*, *39*(20), L20707. https://doi.org/10.1029/2012gl053338

Ye, K., & Messori, G. (2020). Two leading modes of wintertime atmospheric circulation drive the recent warm Arctic–cold Eurasia temperature pattern. *Journal of Climate*, *33*(13), 5565–5587. https://doi.org/10.1175/jcli-d-19-0403.1

Ye, K., & Messori, G. (2021). Inter-model spread in the wintertime Arctic amplification in the CMIP6 models and the important role of internal climate variability. *Global and Planetary Change*, *204*, 103543. https://doi.org/10.1016/j.gloplacha.2021.103543

Ye, K., Woollings, T., & Screen, J. A. (2023). European winter climate response to projected arctic sea-ice loss strongly shaped by change in the North Atlantic Jet. *Geophysical Research Letters*, *50*(5), e2022GL102005. https://doi.org/10.1029/2022gl102005

Ye, K., Woollings, T., Sparrow, S. N., Watson, P. A., & Screen, J. A. (2024). Response of winter climate and extreme weather to projected Arctic sea-ice loss in very large-ensemble climate model simulations. *npj Climate and Atmospheric Science*, *7*(1), 20. https://doi.org/10.1038/s41612-023-00562-5

Zhang, P., Wu, Y., Simpson, I. R., Smith, K. L., Zhang, X., De, B., & Callaghan, P. (2018). A stratospheric pathway linking a colder Siberia to Barents-Kara Sea sea ice loss. *Science Advances*, *4*(7), eaat6025. https://doi.org/10.1126/sciadv.aat6025

Zheng, C., Wu, Y., Ting, M., Screen, J. A., & Zhang, P. (2023). Diverse Eurasian temperature responses to arctic sea ice loss in models due to varying balance between dynamic cooling and thermodynamic warming. *Journal of Climate*, *36*(24), 8347–8364. https://doi.org/10.1175/jcli-d-22-0937.1